SME Annual Meeting
Feb. 27 - Mar. 02, 2022, Salt Lake City, UT

Preprint 22-029

NUMERICAL INVESTIGATION OF THE SIZE EFFECT ON SHALE STRENGTH UNDER UNIAXIAL STRESS STATE

Y. Zhao, West Virginia Univ., Morgantown, WV
B. Mishra, West Virginia Univ., Morgantown, WV
Q. Shi, West Virginia Univ., Morgantown, WV
G. Zhao, West Virginia Univ., Morgantown, WV

ABSTRACT

Shale is anisotropic due to the presence of bedding planes. The anisotropic strength of shale has been extensively studied. However, little attention has been paid to the size effect on shale strength considering the anisotropy. This research uses the discrete element method to study the size effect on the strength of shale under the uniaxial stress state. It is assumed that the anisotropy is caused by bedding planes, while the size effect is caused by randomly distributed flaws. The numerical model of shale comprises three components: shale matrix modeled by bonded particles (2) bedding planes modeled by smooth joints (3) flaws modeled by discrete fractures. The developed model is scaled to different sizes and tested in the uniaxial compression and the direct tension tests. The test result show that the uniaxial compressive strength decreases as the specimen size increases when the loading direction is perpendicular or parallel to bedding planes. The uniaxial compressive strength is determined by the flaws while the bedding planes only play a limited role. However, the size effect on the direct tensile strength depends on the direction of bedding planes. When the loading is perpendicular to bedding planes, the size effect is not prominent. The direct tensile strength is determined by the bedding planes while the flaws have little effect. When the loading direction is parallel to bedding planes, the direct tensile strength decreases when the specimen size increases. The direct tensile strength is determined by the flaws while the bedding planes have little effect.

Keywords: Size effect; Shale; Uniaxial stress state; Transverse isotropy; Discrete element method

INTRODUCTION

The coal mines in the Appalachian region suffer the highest rate of roof fall in the United States (Murphy, 2016). Shale is a leading factor in causing the roof fall since it fails easily under high horizontal stress. (Arora and Mishra, 2015; Bajpayee et al., 2014). To prevent roof failure, it is imperative to know the strength of shale when design the excavation layout and roof support. Measuring the strength in field directly has rarely been conducted due to the high cost of in-situ test (Peng, 2015). Instead, the strength is calculated from laboratory test result according to size effect.

Size effect refers to the influence of size on the mechanical characteristics of material. Hoek and Brown (1980) put forward the most well-known size effect model on the uniaxial compressive strength (UCS) of rock. The Hoek-Brown model presents a reduction of UCS with increasing specimen size and the decrease rate diminishes above a certain size. The Hoek-Brown model is a type of statistical model based on data analysis of published experimental data. Most subsequent researchers dealt with the refinement of the statistical model by using different equations to fit experimental results (Zhang et al., 2011). This situation was changed by the development of fracture mechanics. Bažant (1984) considered the role of fracture energy and proposed the fracture size effect model. Carpinteri et al. (1995) used the concept of geometrical fractal and proposed the multifractal size effect model. These two size effect models show the similar decline trend as the Hoek-Brown model. Furthermore, Bažant (1997) combined the concept of fractal and fracture energy and put forward the fractal fracture size effect model, in which the strength could increase with the increase of size. Moreover, some research show that rock strength increases first and then decreases as size increases (Hawkins, 1998; Masoumi, 2013; Nishimatsu et al., 1969). Therefore, Masoumi et al. (2016) combined the multifractal size effect model and the fractal fracture size effect model to correlate with the ascending and descending trend, and proposed the unified size effect model. In general, the above size effect models are built on the assumption that material contains flaws. Nevertheless, these models neglect the influence of anisotropy, which is critical for some rocks, such as shale.

Shale is made up of several thin laminas that are formed during sedimentary process (O'Brien, 1996). Due to the laminated structure, shale displays fissility as it is ready to split along bedding planes (He and Afolagboye, 2018). Thus, it is relatively strong perpendicular to bedding planes, but considerably weaker parallel to bedding planes (Molinda and Mark, 1996). The anisotropic strength of shale and similar rocks has been studied extensively. Pei (2008) reviewed the uniaxial compression test results and concluded that the maximum value of UCS occurs when the loading direction is parallel or perpendicular to bedding planes, whereas the minimum value occurs when the samples fail along bedding planes. Vervoort et al. (2014) reviewed the Brazilian test results and concluded that the Brazilian tensile strength is maximum when the loading direction is perpendicular to bedding planes and minimum when the loading direction is parallel to bedding planes. Jin et al. (2018) used the direct tensile test and found that the direct tensile strength (DTS) variation is like that of Brazilian tensile strength. In summary, the anisotropy of UCS, Brazilian tensile strength and DTS supports that bedding planes cause the anisotropic strength of shale.

There is very limited work on the combined influence of size effect and anisotropy on the strength of shale or similar rocks. Song et al. (2018) conducted the uniaxial compression test on coal samples and found that the decreasing trend of UCS is greatest when the loading direction is parallel to bedding planes. Li et al. (2021) also found the decreasing trend on the UCS of slate is dependent on the direction of bedding planes. In addition, Li et al. (2020) conducted the Brazilian test on slate and found that the size effect on the Brazilian tensile strength is affected by the anisotropy. When the anisotropy angle is from 45° to 90°, the Brazilian tensile strength increases with specimen size. When the anisotropy angle is from 0° to 30°, the Brazilian tensile strength increases first and then decreases with specimen size. The anisotropy angle is defined as the angle between the loading direction and the normal direction of bedding planes. The size effect study of anisotropic rock is limited due to the great demand of specimen quantity and the size limitation of test frames. However, these difficulties are easily overcome by numerical modeling techniques. In numerical modeling, the challenge is to create the model that incorporates both the size effect and the anisotropy. In the framework of the particle flow code (PFC2D), Park and Min (2015) successfully modeled the anisotropic behavior of rock with smooth joints for representing bedding planes. Zhang et al. (2011) captured the size effect of rock with an embedded discrete fracture network for representing pre-existing flaws. However, rare research has developed the numerical model that includes both the size effect and anisotropy.

The objective of this research is to establish the bonded-particle model of shale which incorporates both size effect and anisotropy. Anisotropy and size effect are assumed to be caused by bedding planes and pre-existing flaws respectively. The bonded-particle model comprises three components: (1) shale matrix modeled by bonded particles (2) bedding planes modeled by smooth joints and (3) flaws modeled by discrete fracturs. The developed model is applied to study the size effect on the strength of shale under the uniaxial stress state.

METHODOLOGY

The bonded-particle model has been widely used to investigate the micromechanical behavior of rock. As for shale, shale matrix is the base material that shows homogeneous and isotropic characteristics. Bedding planes and flaws are viewed as the structural features that cause the anisotropy and the size effect respectively. In the framework of PFC2D, shale matrix, bedding planes and flaws are modeled by bonded particles, smooth joints, and discrete fractures, as shown in **Figure 1**. The modeling techniques of shale matrix, bedding planes, and flaws are discussed in the remaining subsections. The microparameters of shale matrix and bedding planes relevant to the anisotropy of shale are calibrated based on the laboratory test results from (Jin et al., 2018), as listed in **Table 1**. It is important to note that only the results of the anisotropy angle of 0°, 45°, and 90° are considered for the calibration since the size effect study is for the shale with anisotropy angle of 0° and 90°. The microparameters of flaws are calibrated to follow the Hoek-Brown model since it is widely used in the area of rock mechanics.

Table 1. Mechanical properties of shale (Jin et al., 2018).

Anisotropy angle (°)	E (GPa)	UCS (MPa)	DTS (MPa)
0	16.53	61.82	2.73
45	21.18	47.68	4.97
90	36.96	57.39	8.69

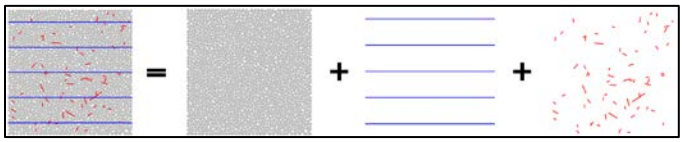

Figure 1. The components parts of shale: shale matrix, bedding planes, and flaws.

MODELING OF SHALE MATRIX

Shale matrix is viewed as an assemblage of granular materials jointed by cementing materials (Potyondy and Cundall, 2004). In PFC2D, the microstructure of the shale matrix is mimicked by particles connected by deformable and breakable bonds as shown in **Figure 2**. The mechanical behavior of the shale matrix is simulated through the deformation and breakage of the bonds. PFC2D provides built-in contact models for simulating the contact mechanism of bonds (Itasca Consulting Group, 2019). The flat-joint model can model the microstructural behaviors of rock during the uniaxial compression and direct tension tests, and can achieve the large UCS/DTS ratio (Potyondy, 2018). The other advantage of the flat-joint model is that the bond interface between each pair of particles can be discretized into elements and each element is either bonded or unbonded (Itasca Consulting Group, 2019). Therefore, the flat-joint model can sustain partial damage. The mechanical behavior of the flat-joint model is described by Potyondy (2016).

The bonded-particle model of shale matrix (BPM-Matrix) was generated following the material-genesis procedure provide by Potyondy (2019). The most important step in the procedure was to assign the microparameters of the BPM-Matrix. These microparameters were obtained through the uniaxial compression test and direct tension test so that the Young's modulus (E), UCS, DTS of the BPM-Matrix match those of shale matrix. The uniaxial compression test and direct tension test were realized in PFC2D as flows: in the uniaxial compression test, a pair of walls were created as the loading platens. In the direct tension test, the surface particles were selected and fixed with velocities to act as the loading platens. The difficulty was how to derive the mechanical properties of the shale matrix from the laboratory test results of shale. Park and Min (2015) recommended that the Young's modulus of shale matrix should be slightly higher (5% used here) than the value of the shale with an anisotropy angle of 90°, which is relatively less affected by the induced fracture along the bedding planes; the UCS and DTS of shale matrix should be selected to be slightly higher (5% used here) than those of shale with the anisotropy angle of 0° and 90° separately. In this paper, the mechanical property of the shale matrix was derived based on the dataset from **Table 1**. After calibration, the mechanical properties of the BPM-Matrix and shale matrix were compared in **Table 2**. The microparameters of the BPM-Matrix were determined in **Table 3**.

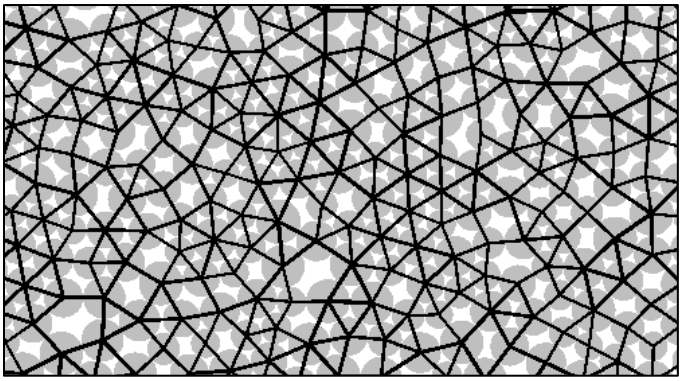

Figure 2. Particles (gray balls) with deformable and breakable bonds (black lines).

Table 2. Mechanical properties of the BPM-Matrix and shale matrix.

Mechanical property	E (GPa)	UCS (MPa)	DTS (MPa)
Shale matrix	38.81	64.92	9.12
BPM-Matrix	38.79	64.89	8.99

Table 3. Microparameters properties of the BPM-Matrix.

Microparameter*	Value
Common group:	
α, C_α, ρ_v[kg/m^3], S_g	0.7, 1, 2558, 0
T_{SD}, $\{D_{\{l,u\}}$[mm], $\phi\}$, D_{mult}	0, {1.0, 1.6, 1.0}, 1.0
Packing group:	
P_m [MPa], ε_P, ε_{lim}	30, 1×10^{-2}, 8×10^{-3},
n_{lim}, C_P, n_c	2×10^6, 1, 0.08
Flat-jointed material group:	
C_{MS}, g$_i$ [mm], ϕ_B, ϕ_G	False, 0.15, 1, 0,
$(g_o)_{\{m,sd\}}$[mm], N_r, $\{C_\lambda, \lambda_v\}$	{0, 0}, 2, {0, 1}
E^*[GPa], κ^*, μ	45, 3.6, 0.4
$(\sigma_c)_{\{m,sd\}}$[MPa]	{13.8, 0}
$(c)_{\{m,sd\}}$[MPa], ϕ[degrees]	{37, 0}, 30
Linear material group:	
E_n^*[GPa], κ_n^*, μ_n	45, 3.6, 0.4

* The microparameters are defined in Potyondy (2019)

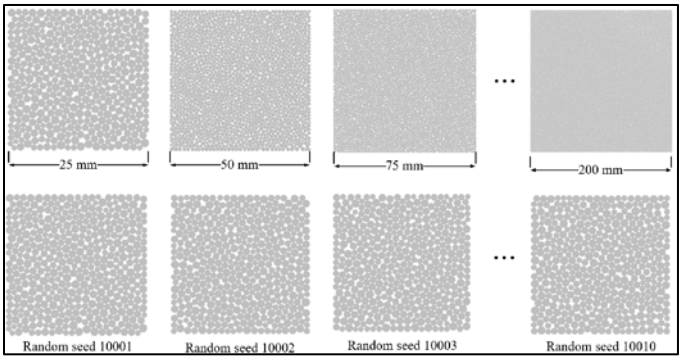

Figure 3. Schematic view of different size BPM-Matrix models and their 10 realizations.

From the introduction section, it is widely acknowledged that the size effect of rock is caused by the existence of flaws. Before

introducing flaws, we verified the presupposition that there is no size effect for the shale matrix. The verification was accomplished by testing the BPM-Matrix at different sizes and comparing their mechanical properties. However, the packing arrangement of particles is different in different-size models (Potyondy and Cundall, 2004). The change of packing arrangement will influence the mechanical properties. Therefore, the influence of packing arrangement was eliminated before comparing different size models. This was accomplished by creating several models for each size and using the average value of the test results. In this paper, the models with the size of 25 mm, 50 mm, 75 mm, 100 mm, 125 mm, 150 mm, and 200 mm were selected. 10 realizations for each model size were created by varying the random seed in the material genesis stage. **Figure 3** shows the schematic view of 7 different sizes models and their 10 realizations. The first row shows the BPM-Matrix varying in size with the same random seed as 10001. The second row shows the BPM-Matrix varying in packing arrangement with the same size as 25 mm.

Seventy models were tested in the uniaxial compression and direct tension test. **Figure 4** shows the test result of UCS and DTS. The change of packing arrangement results in scattered results of UCS and DTS at each size. The scatter of UCS and DTS exhibits no clear change with increasing model size. This result is different from the work of Koyama and Jing (2007), in which the scatter decreases with increasing model size. The reason might be the use of different material genesis procedure. In addition, the size effect on UCS and DTS is different. The average value of UCS is nearly constant when the model size changes except for a small increase at the size of 25 mm. However, the average value of DTS decreases from 9 MPa to 6.5 MPa as the model size increases and the decrease rate is constant. The result of UCS satisfies the presupposition, but the result of DTS is contrary to the presupposition.

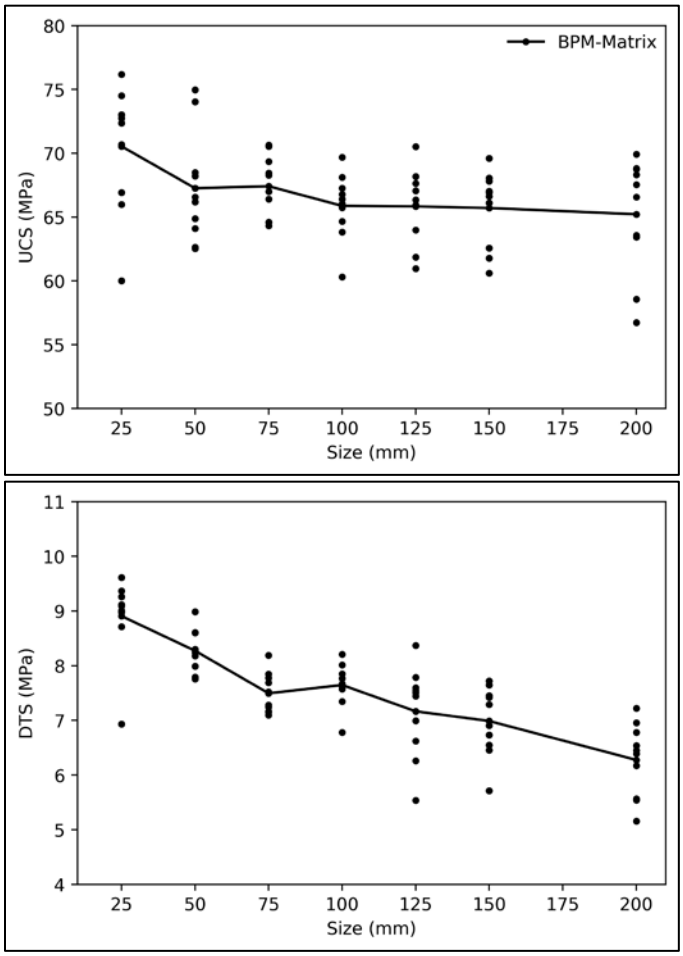

Figure 4. Size effect on the UCS and DTS of BPM-Matrix.

MODELING OF BEDDING PLANES

Bedding planes are generally weaker compared to shale matrix. They have lower strength and higher compressibility, and contribute significantly to the anisotropy of shale (Park and Min, 2015). In the bonded-particle model, smooth joints can simulate the mechanical behavior of bedding planes. Smooth joints are added into BPM-Matrix by replacing the flat-joint model between particles with the smooth-joint contact model, as shown in **Figure 5**. The smooth-joint model can overcome the inherent roughness problem of particles. It can simulate the behavior of a bedding plane by forcing the contacting surfaces of particles to align with the plane, thus the particles that lie on opposite sides of the joint can slide past one another instead of over-riding one another (Itasca Consulting Group, 2019). Deisman (2008) provided a detailed description of the smooth-joint model. The calibration of the bonded-particle model with smooth joints (BPM-Joint) is more complicated than BPM-Matrix due to the anisotropic behavior of shale. Thus, three BPM-Joint models with the anisotropy angle as 0°, 45°, and 90° were created for calibration. The calibrated model size was selected as 50 mm and the joint spacing was selected as 10 mm. After calibration, the mechanical properties of the bonded-particle model with smooth joints (BPM-joint) matched those of shale, as listed in **Table 4**. **Table 5** shows the microparameters of the smooth-joint model.

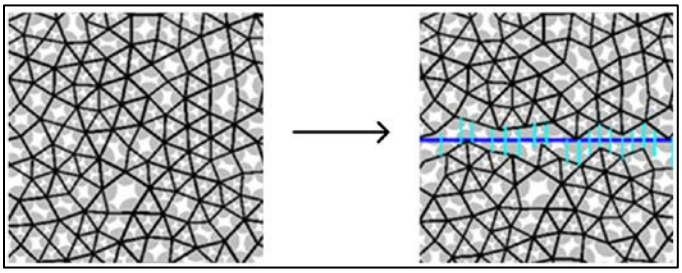

Figure 5. Smooth joints overlaid on the BPM-Matrix (with particles in gray, flat-joint contact in black, bedding planes in blue and smooth-joint contacts in aqua).

Table 4. Mechanical properties of the BPM-Joint and shale.

Anisotropy angle (°)		E (GPa)	UCS (MPa)	DTS (MPa)
0	Shale	16.53	61.82	2.73
	BPM-Joint	16.46	61.47	2.78
45	Shale	21.18	47.68	4.97
	BPM-Joint	22.42	47.90	4.59
90	Shale	36.96	57.39	8.69
	BPM-Joint	36.37	54.20	8.71

Table 5. Microparameters of the smooth joint model.

Microparameter	Value
Normal stiffness (GPa/m)	1,750
Shear stiffness (GPa/m)	1,750
Friction coefficient	0.4
Friction angle (°)	30
Tensile strength (MPa)	2.2
Cohesion (MP)	13.5

After adding smooth joints into the bonded-particle model, we verified that there is no size effect for the BPM-Joint model. The BPM-Joint models were tested in two directions, the load is parallel or perpendicular to bedding planes (anisotropy angles are 0° and 90° separately). The test plan of BPM-Joint was the same as BPM-Matrix. It contained 7 different size models and 10 realizations for each size, as shown in **Figure 6**. The test results of the uniaxial compressive strength and direct tensile strength are shown in **Figure 7**. For the convenience of comparison, the result of BPM-Matrix is also included.

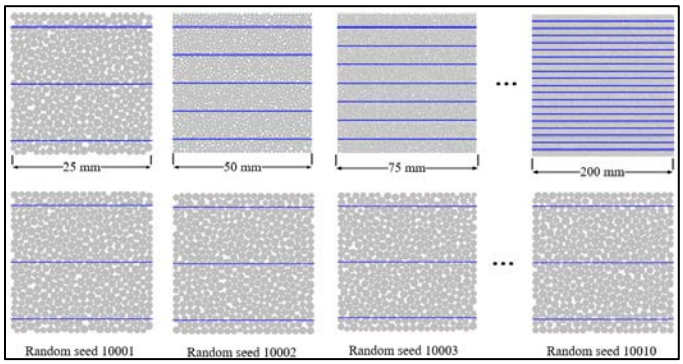

Figure 6. Schematic view of different size BPM-Joint models and their 10 realizations.

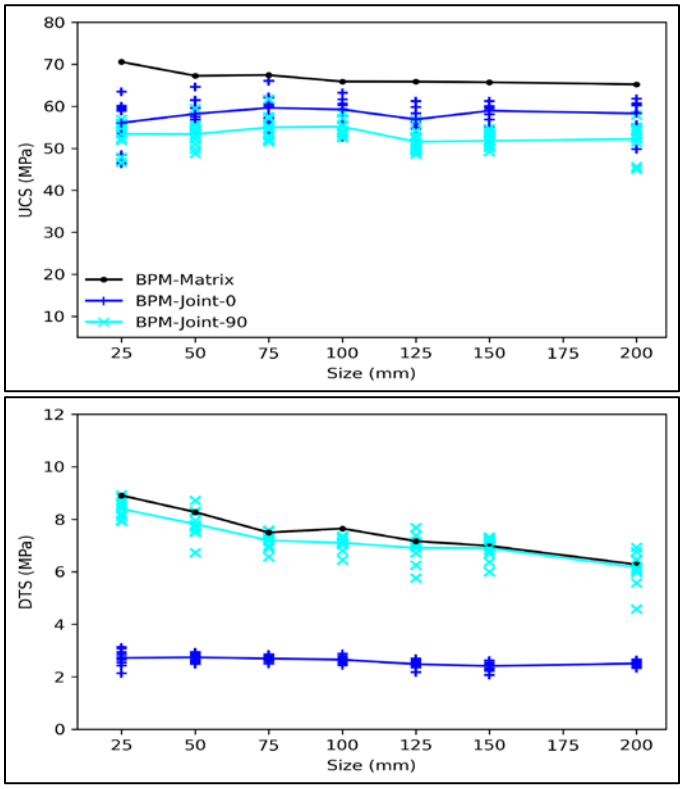

Figure 7. Size effect on the UCS and DTS of BPM-Joint and BPM-Matrix.

Figure 7 shows that the UCS and DTS of BPM-Matrix are higher than those of BPM-Joint regardless of the anisotropy angle. This result demonstrates that bedding planes are planes of weakness. The UCS and DTS of BPM-Joint with the anisotropy angle of 0° (BPM-Joint-0) are always higher than BPM-Joint with the anisotropy angle of 90° (BPM-Joint-90). It verifies that the bedding plane causes the anisotropy behavior of shale. As for the size effect, the UCS of BPM-Joint-0 and BPM- Joint-90 is nearly constant when the model size increases, which is very similar to BPM-Matrix. Thus, there is no size effect on the UCS of BPM-Joint when the anisotropic angle is 0° or 90°. The size effect on DTS of BPM-Joint-90 shows a declining trend which is nearly the same as that of BPM-Matrix. However, the DTS of BPM-Joint-0 is constant with the increasing model size. Besides, the DTS scatter of BPM-Joint-0 is smaller than BPM-Joint-90. The DTS difference is caused by the failure pattern. When the direct tensile load is perpendicular to the bedding planes, the DTS of BPM-Joint is controlled by the tensile strength of bedding planes. The DTS is around 2.5 MPa regardless of the change of model size. When the direct tensile load is parallel to the bedding planes, the DTS is determined by the strength of BPM-Matrix which shows a declining size effect. In conclusion, there is no size effect on the UCS of BPM-Joint-0 or BPM-Joint-90, and the DTS of BPM-Joint-0. But there is a reduction on the DTS of BPM-Joint-0, which should be considered in the latter size effect analysis.

Modeling of flaws

There is no size effect on the UCS of BPM-Matrix and BPM-Joint in the previous result. Based on assumption that the size effect is caused by the existence of flaws, our next step is to introduce flaws. Flaws can be added upon the BPM-Matrix so that the composite model (BPM-Flaw) could capture the Hoek-Brown size effect model. In the bonded particle model, flaws are generated through the discrete fracture network technique (Cundall et al., 2008). To properly generate flaws, the mechanical behavior and spatial distribution of flaws were obtained in advance. Council (1996) defined flaws as mechanical breaks in rocks. In the bonded-particle model, the mechanical behavior of flaws was realized by changing the status of the flat-joint contact from bonded to unbonded, as shown in **Figure 8**. Thus, flaws inherited the same microparameters from the shale matrix except that the tensile strength and cohesion were set as 0.

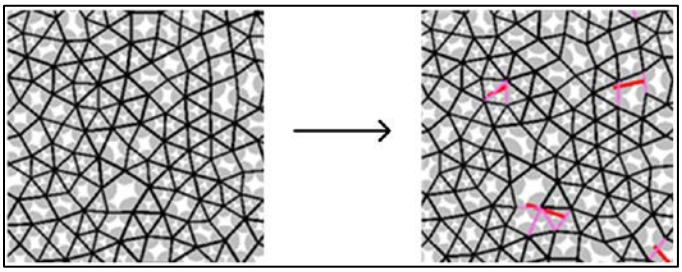

Figure 8. Flaws overlaid on the BPM-Matrix (with particles in gray, flat-joint bonds in black, flaws in red and broken bonds in violet)

As for the geometrical properties, the position and orientation of flaws were assumed to be randomly distributed in the shale matrix according to the work (Zhang et al., 2011). The flaw size and density were assumed to follow the power-law distribution (Bonnet et al., 2001). The relationship is

$$n(l) = \alpha \times l^{-c}$$

where l is the flaw size, $n(l)$ is the number of flaws with the size is in the range $[l,\ l+dl]$, α is the density constant, and c is the scaling exponent. The distribution of flaw size is between the lower bound l_{min} and upper bound l_{max}. An example of the power-law distribution is shown in **Figure 9**. It shows that the scaling exponent $-c$ is the slope of the line. When c increases, the proportion of small flaws will increase relative to large flaws. **Table 6** presents the parameters of the power-law distribution. The value of l_{min} was set as the smallest size of particles, since the smallest flaw exists between the exact one pair of particles. l_{max} was set as the model size of the shale matrix which indicates that the larger model is more likely to contain large flaws. The value of α and c were calibrated so that the BPM-Flaw can capture the decreasing size effect.

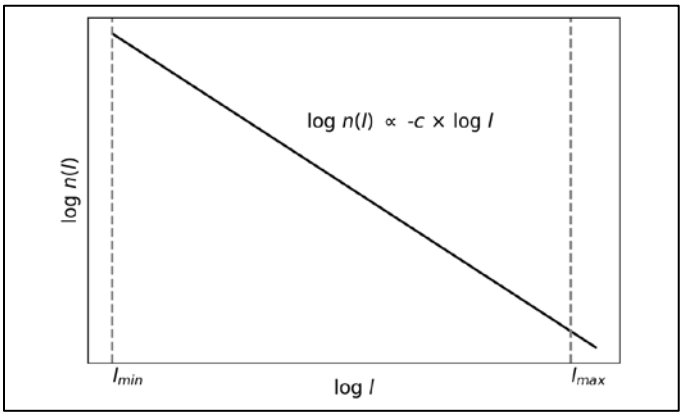

Figure 9. The power-law distribution of flaw size in log-log diagram.

Table 6. Parameters of the power-law distribution of flaw size.

Parameter	α (mm/mm^2)	c	l_{min} (mm)	l_{max} (mm)
Value	5000	3	1	Specimen size

Figure 10 shows the 7 different-size BPM-Flaw and their 10 realizations. The test results of BPM-Flaw are shown in **Figure 11**. The result of BPM-Matrix is included for the convenience of comparison. The UCS and DTS of BPM-Flaw are lower than those of BPM-Matrix. There is a significant decreasing size effect on UCS for BPM-Flaw compared with BPM-Matrix. The decreasing trend of UCS is very close to the Hoek-Brown model. The UCS decreases from 45 MPa to 30 MPa when the specimen size increases from 25 mm to 125 mm. The decrease rate of UCS diminishes when the specimen size is above 125 mm. Besides, the scatter of UCS seems to decrease with the increasing specimen size. Thus, we can conclude that the introduction of flaws successfully captured the decreasing size effect on UCS. However, the effect of flaws on DTS is not obvious. The DTS reduction of BPM-Flaw is very similar to BPM-Matrix. But the decrease rate of DTS for BPM-Flaws diminishes when the specimen size is above 125 mm.

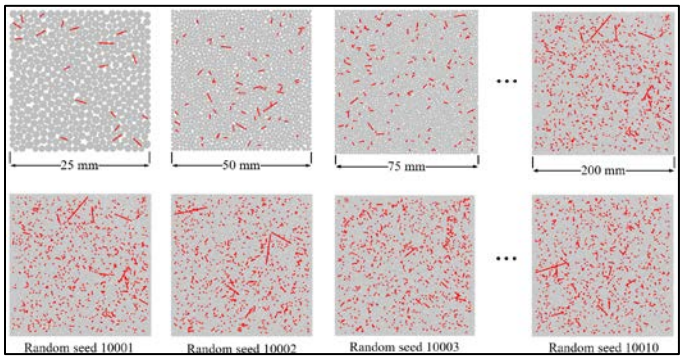

Figure 10. Schematic view of different size BPM-Flaw models and their 10 realizations.

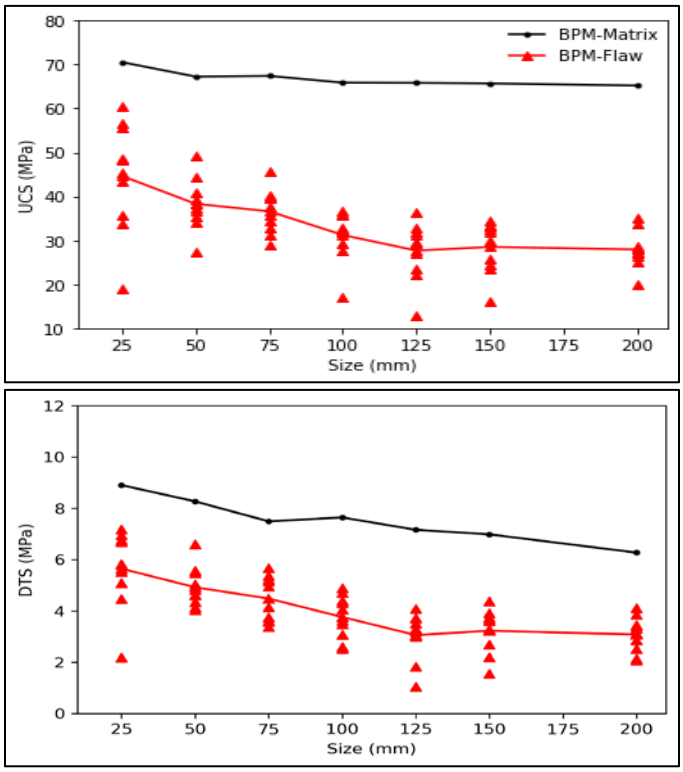

Figure 11. Influence of model size on UCS and DTS of different models.

SIZE EFFECT ON THE UCS AND DTS OF SHALE

The bonded-particle model of shale (BPM-Shale) was established by assembling the components: shale matrix, bedding planes, and flaws. **Figure 12** presents the different-size BPM-Shale with the anisotropy angles of 0° and 90°. The model of each size has 10 realizations.

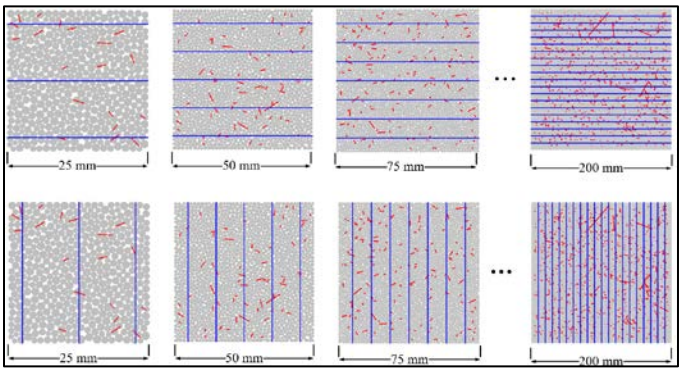

Figure 12. Schematic view of different size BPM-Shale models with the anisotropy angles of 0° and 90°.

Figure 13 shows the results of UCS and DTS of the BPM-Shale. The results are compared with those of BPM-Joint. From **Figure 13**, there is no size effect on the UCS for BPM-Joint with the anisotropy angle of 0° or 90°. After the introduction of flaws, the UCS of BPM-Shale shows declining trend with increase in the model size. The decrease rate diminishes when the model size is above 125 mm. This result demonstrated that the size effect is caused by the flaws. The UCS difference between BPM-Shale-0 and BPM-Shale-90 is nearly the same as that of BPM-Joint-0 and BPM-Joint-90, and the difference shows the anisotropic strength of BPM-Shale. However, the UCS difference between BPM-Shale and BPM-Joint is relatively large. This result demonstrates that the UCS of BPM-Shale is controlled by the flaws while the bedding planes only play a limited role. The size effect on the DTS is different. When the anisotropy angle is 0°, there is no size effect on the DTS of BPM-Joint. However, the DTS of BPM-Shale shows a slight strength reduction with the increasing specimen size.

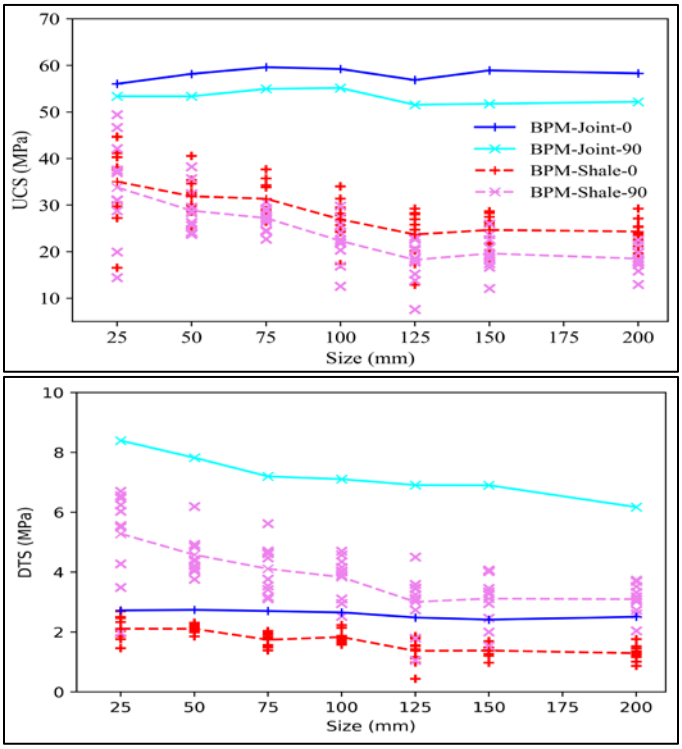

Figure 13. Size effect on the UCS and DTS of BPM-Shale.

This slight strength reduction is caused by the flaws. This result demonstrates that the DTS is mainly determined by the bedding planes and the flaws have little influence. When the anisotropy angle is 90°, the DTS of BPM-Shale shows a similar declining trend as that of BPM-Joint. But the decrease rate diminishes when the specimen size is above 125 mm. The DTS difference between BPM-Shale-90° and BPM-Joint-90° is relatively larger than the difference between BPM-Shale-0° and BPM-Joint-0°. It demonstrates that the DTS is controlled by flaws rather than bedding planes.

CONCLUSION

The size effect of shale was numerically investigated using the discrete element method. The bonded-particle model of shale was created in PFC2D to incorporate both the transverse isotropy and size effect. The anisotropy was modeled by the bonded-particle model with embedded smooth joints while the size effect was introduced by randomly distributed flaws. The numerical models were then scaled and tested in the uniaxial compression test and direct tension test. The main conclusions are summarized as follows.

The UCS of the shale model decreases when the model size increases regardless of the loading direction is perpendicular or parallel to bedding planes. The UCS is controlled by the flaws while the bedding planes only play a limited role. However, the size effect on the DTS is more complicated. When the loading direction is perpendicular to bedding planes, there is a slight reduction of the DTS, and the DTS is mainly controlled by the bedding planes rather than flaws. When the loading direction is parallel to bedding planes, the DTS decreases when the model size increases. The DTS is controlled by the flaws rather than bedding planes.

REFERENCES

1. Arora, S., Mishra, B., 2015. Investigation of the failure mode of shale rocks in biaxial and triaxial compression tests. Int. J. Rock Mech. Min. Sci. 79, 109–123.
2. Bajpayee, T.S., Pappas, D.M., Ellenberger, J.L., 2014. Roof Instability: What Reportable Noninjury Roof Falls in Underground Coal Mines Can Tell Us. Prof. Saf. 59, 57–62.
3. Bažant, Z.P., 1997. Scaling of quasibrittle fracture: hypotheses of invasive and lacunar fractality, their critique and Weibull connection. Int. J. Fract. 83, 41.
4. Bažant, Z.P., 1984. Size effect in blunt fracture: concrete, rock, metal. J. Eng. Mech. 110, 518–535.
5. Carpinteri, A., Chiaia, B., Ferro, G., 1995. Size effects on nominal tensile strength of concrete structures: multifractality of material ligaments and dimensional transition from order to disorder. Mater. Struct. 28, 311.
6. Deisman, N., Ivars, D.M., Pierce, M., 2008. PFC2D Smooth joint contact model numerical experiments. Proc. GeoEdmonton'08, Pap. 83, Edmonton, Canada.
7. Hawkins, A.B., 1998. Aspects of rock strength. Bull. Eng. Geol. Environ. 57, 17–30.
8. He, J., Afolagboye, L.O., 2018. Influence of layer orientation and interlayer bonding force on the mechanical behavior of shale under Brazilian test conditions. Acta Mech. Sin. 34, 349–358.
9. Hoek, E., Brown, E.T., 1980. Underground excavations in rock. CRC Press.
10. Itasca Consulting Group, I., 2019. PFC | US Minneapolis.
11. Jin, Z., Li, W., Jin, C., Hambleton, J., Cusatis, G., 2018. Anisotropic elastic, strength, and fracture properties of Marcellus shale. Int. J. Rock Mech. Min. Sci. 109, 124–137.
12. Koyama, T., Jing, L., 2007. Effects of model scale and particle size on micro-mechanical properties and failure processes of rocks-A particle mechanics approach. Eng. Anal. Bound. Elem. 31, 458–472.
13. Li, K., Cheng, Y., Yin, Z.Y., Han, D., Meng, J., 2020. Size Effects in a Transversely Isotropic Rock Under Brazilian Tests: Laboratory Testing. Rock Mech. Rock Eng. 53, 2623–2642.
14. Li, K., Yin, Z.-Y., Han, D., Fan, X., Cao, R., Lin, H., 2021. Size Effect and Anisotropy in a Transversely Isotropic Rock Under Compressive Conditions. Rock Mech. Rock Eng.
15. Masoumi, H., 2013. Investigation into the mechanical behaviour of intact rock at different sizes. Dr. Philos. thesis, Univ. New South Wales, Sydney.
16. Masoumi, H., Saydam, S., Hagan, P.C., 2016. Unified size-effect law for intact rock. Int. J. Geomech. 16, 1–15.
17. Molinda, G.M., Mark, C., 1996. Rating the strength of coal mine roof rocks. Information circular ;9444.
18. Murphy, M.M., 2016. Shale Failure Mechanics and Intervention Measures in Underground Coal Mines: Results From 50 Years of Ground Control Safety Research. Rock Mech. Rock Eng. 49, 661–671.
19. Nishimatsu, Y., Yamaguchi, U., Motosugi, K., Morita, M., 1969. The size effect and experimental error of the strength of rocks. J Min Mat Proc Inst Jpn 18, 1019–1025.
20. O'Brien, N.R., 1996. Shale lamination and sedimentary processes. Geol. Soc. London, Spec. Publ. 116, 23–36.
21. Park, B., Min, K.B., 2015. Bonded-particle discrete element modeling of mechanical behavior of transversely isotropic rock. Int. J. Rock Mech. Min. Sci. 76, 243–255.
22. Park, B., Min, K.B., Thompson, N., Horsrud, P., 2018. Three-dimensional bonded-particle discrete element modeling of mechanical behavior of transversely isotropic rock. Int. J. Rock Mech. Min. Sci. 110, 120–132.
23. Pei, J., 2008. Strength of Transversely Isotropic Rocks. M.S., Civ. Environ. Eng. Massachusetts Inst. Technol.
24. Peng, S.S., 2015. Topical areas of research needs in ground control--a state of the art review on coal mine ground control. Int. J. Min. Sci. Technol. 25, 1–6.
25. Potyondy, D., 2019. Material-modeling support in PFC [fistpkg6.6]. Itasca Consult. Group, Inc., Minneapolis, Minnesota, Tech. Memo. ICG7766-L (December 11, 2019).
26. Potyondy, D.O., 2018. A flat-jointed bonded-particle model for rock. 52nd U.S. Rock Mech. Symp.
27. Potyondy, D.O., 2016. Flat-joint contact model [version 1], Itasca Consulting Group, Inc.
28. Potyondy, D.O., Cundall, P.A., 2004. A bonded-particle model for rock. Int. J. Rock Mech. Min. Sci. 41, 1329–1364.
29. Song, H., Jiang, Y., Elsworth, D., Zhao, Y., Wang, J., Liu, B., 2018. Scale effects and strength anisotropy in coal. Int. J. Coal Geol. 195, 37–46.
30. Vervoort, A., Min, K.B., Konietzky, H., Cho, J.W., Debecker, B., Dinh, Q.D., Frühwirt, T., Tavallali, A., 2014. Failure of transversely isotropic rock under Brazilian test conditions. Int. J. Rock Mech. Min. Sci. 70, 343–352.
31. Zhang, Q., Zhu, H., Zhang, L., Ding, X., 2011. Study of scale effect on intact rock strength using particle flow modeling. Int. J. Rock Mech. Min. Sci. 48, 1320–1328.